Optics Communications 291 (2013) 380–385

Contents lists available at SciVerse ScienceDirect

Optics Communications

journal homepage: www.elsevier.com/locate/optcom

# Hybrid photonic–plasmonic mode for refractometer and nanoparticle trapping

Yi-Wen Hu, Bei-Bei Li, Yi-Xiang Liu, Yun-Feng Xiao*, Qihuang Gong*

*State Key Laboratory for Mesoscopic Physics, School of Physics, Peking University, Beijing 100871, People's Republic of China*

ARTICLE INFO

*Article history:*
Received 8 August 2012
Received in revised form
28 October 2012
Accepted 3 November 2012
Available online 29 November 2012

*Keywords:*
Hybrid photonic–plasmonic mode
Microdisk cavity
Refractometer
Nanoparticle trapping

ABSTRACT

We theoretically study hybrid photonic–plasmonic modes in a composite structure in which a silicon microdisk is vertically coupled to a metal microdisk. Benefitting from the low-loss property of whispering gallery modes and the strong field localization of plasmonic modes, the hybrid modes hold potential advantages over conventional photonic or plasmonic devices, in particular toward sensing and nanoparticle trapping. In the refractometer application, a high figure of merit exceeding 200 can be obtained in 1550 nm wavelength band. In the nanoparticle trapping, the composite structure enables a significant power enhancement in the hybrid mode, and the gradient force reaches as high as 48 pN/W for a single polystyrene nanoparticle with a radius of 5 nm. Since the enhanced gradient force pulls the nanoparticles into the area with the strongest electromagnetic field, this composite device is beneficial to nanoparticle detection with low noise and fast response.



## 1. Introduction

Optical microcavities with both high quality factor $Q$ and small mode volume $V$ are of great importance since they provide an excellent platform to study strong light–matter interaction [1]. For example, high $Q/V$ microcavities show great potential for optical biosensing applications [2–7]. On one hand, conventional dielectric cavities can achieve ultrahigh $Q$, but their physical sizes cannot be smaller than the wavelength scale due to diffraction limit. On the other hand, surface plasmonic polariton (SPP) devices, which exploit collective oscillations of electron gas coupled with optical waves, can break through the diffraction limit and achieve tight confinement of electromagnetic field, whereas huge intrinsic loss of metal limits the $Q$ factor. As a result, many efforts have been made to combine the advantages of the above two kinds of devices [8–13]. Among these studies, metal nanostructures (typically nanoparticles) are placed in an optical cavity to create a hybrid photonic–plasmonic mode. The hybrid mode can generate a hotspot of high field intensity without significantly degrading $Q$ factor [14].

Recently, another type of hybrid mode is attracting much attention. For the plasmonic part, unlike previous hybrid devices mostly using metal particles, it adopts bulk metal materials such as metal substrate, metal strip or metal microcavity to support hybrid mode. For the photonic part, both waveguide modes [15–20] and optical whispering-gallery modes (WGMs) [21–23] can be employed. Importantly, this type of device is very promising to be integrated on a chip due to fabrication compatibility. Biochemical sensors based on this hybrid mode are reported and they exhibit main advantages of small footprint and high sensitivity [24–27]. However, a detailed analysis of the optical trapping force in this kind of hybrid mode, which is important for sensing applications is still lacking.

Here we propose a hybrid photonic-plasmonic device formed by a silver microdisk fabricated on a silicon disk with tens of nanometers gap between them. A refractometer (RI) sensor with high sensitivity larger than 200 nm per refraction index unit (RIU) and high figure of merit (FOM) exceeding 200 is realized based on it. Moreover, the optical force induced by the strong light intensity is analyzed, and the results demonstrate that the gradient force reaches as high as 48 pN/W for a 5 nm radius PS particle, which is one order of magnitude larger than that of previous hybrid plasmonic structures [20] because of field enhancement. As a result, this structure can effectively drag nanoparticles into the gap region with the strongest field intensity and is beneficial to the nanoparticle detection with low noise and fast response. In addition, we study the possible application of controlling the trapping position of the nanoparticles by exciting different radial order modes. In the last section we discuss the viability of exciting this hybrid mode with an access waveguide, which can be integrated on a microfluidic chip. Our study implies an optimistic future of this hybrid photonic-plasmonic mode to be applied in the nanoparticle sensor or tweezer.

* Corresponding authors. Tel.: +86 10 62765512.
*E-mail addresses:* yfxiao@pku.edu.cn (Y.-F. Xiao), qhgong@pku.edu.cn (Q. Gong).

0030-4018/$ - see front matter © 2012 Elsevier B.V. All rights reserved.
http://dx.doi.org/10.1016/j.optcom.2012.11.024

## 2. Device structure

The proposed composite structure consists of a silver microdisk vertically coupled with a silicon microdisk, as shown in Fig. 1(a). By using finite element method (FEM) simulation, we obtain the field intensity $|\boldsymbol{E}|^2$ distributions for different modes around 1550 nm, shown in Fig. 1(b)–(e). We can find from Fig. 1(b) and (c) that the hybridization of quasi-TE modes is much better than that of quasi-TM modes. This is because the electric field at the interface is perpendicular to the metal surface, which matches well with quasi-TE-polarized WGMs. In the following, we thus focus on the analysis of quasi-TE modes. As a result of the hybridization of SPP and WGM modes, large energy is confined within the nanometer-scaled gap, providing an efficient way for RI sensing and nanoparticle trapping. In Fig. 1(d) and (e), high-order radial hybrid modes ($\upsilon=2$) are displayed. It can be seen that multiple trapping hot spots can form in high order modes, which may be applied in controlling the trapping position of the nanoparticles and will be discussed in Section 4. Finally, we point out that by using an SOI wafer, the fabrication of this structure is compatible with the standard CMOS microelectronics technology. To support a silver microdisk above, first grow an oxidation layer on the silicon cavity, and then the oxidation layer can be partially etched to form a supporting pillar after the silver microdisk is fabricated. As a result, the oxidation layer thickness just determines the gap size $g$ between silicon and silver.

The $Q$ factor, associated with the photon lifetime and the power enhancement factor $G$, is one of the most important parameters for microresonators. In this hybrid structure, the loss is dominated by the metal absorption, since it is much larger than that of silicon and the gap (air or water). This means lesser the energy distributed in the metal, smaller the total loss. Owing to the hybridization of the WGM and SPP modes, little energy is distributed in the metal. For example, for the modes in Table 1, ~20% energy distributes within the gap and ~75% energy in silicon. Thus only ~5% energy distributes in the metal, greatly suppressing the loss from the metal absorption. Consequently the $Q$ factor of the hybrid mode is larger than that of conventional SPP microresonators. This can also be verified by calculating the propagation length $L_m$ ($L_m=1/\alpha$, with $\alpha$ being the optical loss coefficient) of the hybrid mode, as shown in Table 1. The results show that, for the hybrid mode, $L_m$ is around 150–200 μm, much larger than that of conventional SPP modes [15]. Furthermore, compared with hybrid plasmonic waveguide, the cavity structure can provide a power enhancement effect. The enhancement factor $G$ can be obtained as

$$G=1+e^{-\alpha L}+e^{-2\alpha L}+\cdots=\frac{1}{1-e^{-\alpha L}}=\frac{1}{1-e^{-2\pi m/Q}} \quad (1)$$

where $\alpha$, $m$, and $L$ represent the optical loss coefficient, the azimuthal mode number, and the circumference of the cavity respectively. Here we have utilized $m\lambda=2\pi nR$ with $n$ and $R$ being the effective refractive index and the radius of the microresonators, respectively.

In this paper we focus on the cavity mode near 1550 nm telecommunication waveband (Table 1). The largest $Q$ ($G$) is around 2000 (10), both of which exceed those of traditional plasmonic resonators. Specifically, for this hybrid photonic-plasmonic mode, $Q$ is mainly limited by the radiation loss for small microresonators, so $Q$ increases with radius going up, and levels off when $R>4$ μm because in this range, $Q$ is not limited by the radiation loss but the metal absorption loss, which does not change much with increasing $R$. The power enhancement $G$, depending on both $R$ and $Q$, decreases monotonously with increasing $R$, indicating that in this structure, smaller radius brings about stronger light enhancement.

Now we turn to consider other parameters influencing the device properties, such as the thickness of silicon layer $H_{Si}$ and the gap $g$, which affect the coupling between WGM and SPP modes. In Fig. 2(a), when $H_{Si}$ increases, less evanescent field can leak into the gap region, thus leading to a smaller energy fraction in liquid $\eta$ ($\eta=P_{liquid}/(P_{liquid}+P_{Ag}+P_{Si}$ where $P_{liquid}$, $P_{Ag}$, and $P_{Si}$ denote the

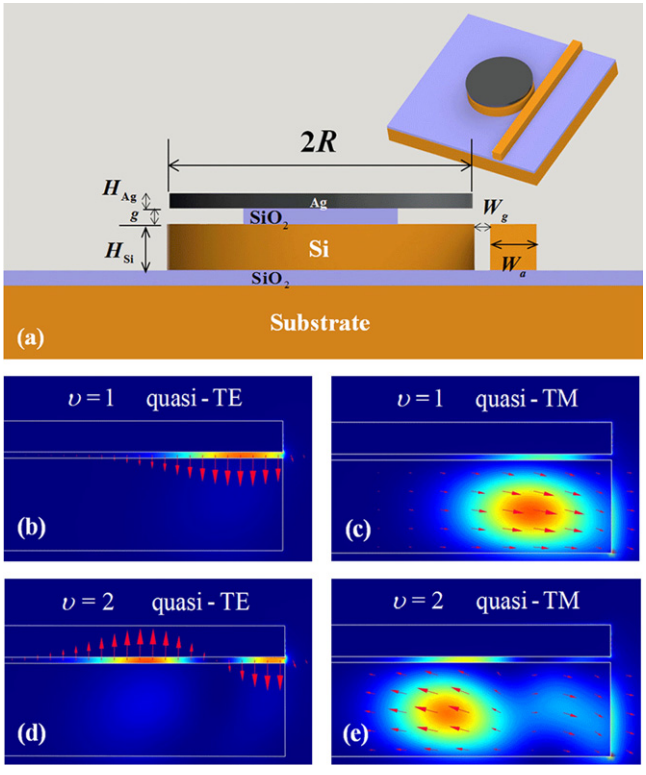


**Fig. 1.** (a) Schematic configuration of the hybrid photonic-plasmonic microdisk coupled with a waveguide. (b)–(e) Field distributions ($|\boldsymbol{E}|^2$) for quasi-TE and TM modes around 1550 nm. The size parameters of this structure are set as follows: $R=2$ μm, $H_{Ag}=100$ nm, $g=20$ nm,and $H_{Si}=300$ nm. The permittivities are $\varepsilon_1=-129+3.3i$ for silver, $\varepsilon_2=1.7689$ for the surrounding liquid (water), and $\varepsilon_3=12.25$ for silicon. The red arrows denote the directions of local electric fields. (For interpretation of the references to color in this figure legend, the reader is referred to the web version of this article.)

**Table 1**
Calculated $Q$ factor, propagation length $L_m$ and power enhancement factor $G$ for different fundamental modes (only quasi-TE modes are considered) with increasing $R$. The parameters are: $H_{Ag}=100$ nm, $H_{Si}=300$ nm and $g=20$ nm.

| $R$ (μm) | $m$ | $\lambda$ (nm) | $Q$ | $L_m$ (μm) | $G$ |
|---|---|---|---|---|---|
| **1** | 9 | 1538 | 708 | 79 | 13 |
| **2** | 19 | 1587 | 1227 | 129 | 10 |
| | 20 | 1524 | 1437 | 144 | 11 |
| **3** | 30 | 1573 | 1454 | 145 | 7.7 |
| | 31 | 1534 | 1660 | 161 | 8.5 |
| **4** | 41 | 1573 | 1765 | 172 | 6.9 |
| | 42 | 1545 | 2161 | 206 | 8.2 |
| **5** | 52 | 1571 | 1725 | 166 | 5.3 |
| | 53 | 1548 | 1699 | 160 | 5.1 |
| **6** | 64 | 1555 | 1635 | 153 | 4.1 |
| | 65 | 1536 | 1696 | 157 | 4.2 |
| **7** | 75 | 1561 | 1616 | 151 | 3.4 |
| | 76 | 1544 | 1676 | 154 | 3.5 |
| **8** | 87 | 1551 | 1669 | 153 | 3.1 |
| | 88 | 1537 | 1727 | 157 | 3.1 |
| **9** | 98 | 1557 | 1657 | 152 | 2.7 |
| | 99 | 1544 | 1709 | 155 | 2.7 |
| **10** | 109 | 1561 | 1659 | 152 | 2.4 |
| | 110 | 1550 | 1706 | 155 | 2.5 |

EM energy in liquid, silver and silicon, respectively) but a better cavity finesse $F$ as more fraction of field is concentrated in the low-loss dielectric area. In Fig. 2(b), it is not a surprise to find a similar trend for $F$ as a larger $g$ also weakens the influence of metal absorption loss. For $\eta$, however, the maximum value occurs around $g=14$ nm. This is because when $g$ is large, the cavity tends to form a pure WGM and little field distributes outside the silicon disk, while when $g$ is too small, the limited size gap region also brings down $\eta$.

For sensing applications, one important parameter is the sensitivity $S$, defined as $S=\delta\lambda/\delta n$, which is proportional to the energy fraction $\eta$ in liquid [28], so $S$ decreases with $H_{Si}$ reducing. The optimized $S$ can be obtained when $g=14$ nm. Another key parameter is the detection limit (DL) which is determined by the product of $F$ and $\eta$ ($DL\propto\Delta\lambda/S\propto\lambda/F\eta$). It can be inferred from the data in Fig. 2 that $H_{Si}$ and $g$ should be as large as possible to get a small DL. However, large $H_{Si}$ and $g$ will sacrifice the sensitivity, leading to a low signal-to-noise ratio (SNR), which is also important in practical sensing applications. In the next section, $H_{Si}$ ($g$) is chosen as 300 nm (20 nm) to realize a balance between sensitivity and detection limit.

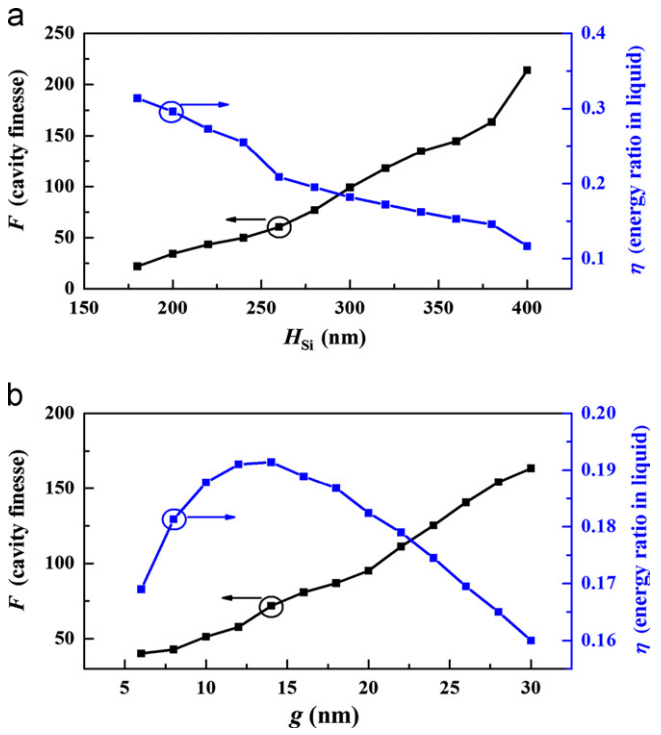


**Fig. 2.** Cavity finesse $F$ and energy fraction $\eta$ in liquid with (a) increasing $H_{Si}$ and fixed $g=20$ nm, and (b) increasing $g$ and fixed $H_{Si}=300$ nm. Other cavity and mode parameters are set as follows: $H_{Ag}=100$ nm, $R=1$ μm, and the corresponding mode numbers are $m=9$ and $\upsilon=1$. In this figure, we see that there exists a tradeoff between $F$ and $\eta$, so $H_{Si}$ and $g$ are chosen as 300 nm and 20 nm, respectively, in the sensing analysis in the next section.

## 3. Hybrid plasmonic refractometer

For our hybrid mode, much energy is confined in the gap region, in which we can fill with the liquid to be detected, thus the sensitivity can be enhanced when utilized as a sensor. Now we consider the performance of this hybrid mode for RI sensing application. The size parameters are set as $H_{Ag}=100$ nm, $g=20$ nm and $R=10$ μm.

The sensitivity $S$ and detection limit DL represent the two key parameters in characterizing an optical sensor. The detection limit is the smallest detectable RI change, which can also be described by figure of merit (FOM), defined as $FOM=SQ/\lambda$. Then we quantify the sensing performance of this hybrid mode by analyzing $S$ and FOM. The sensitivity $S=\delta\lambda/\delta n_2$, where $n_2$ denotes the refractive index of the liquid to be detected filled in the gap area. By changing $n_2$ and calculating the resonant wavelength, we can derive $S$. As shown in Fig. 3, a very good linear dependence of the resonance wavelength on $n_2$ is exhibited. The sensitivity of 208 nm/RIU is achieved in 1550 nm band. With $Q$ being 1700, the FOM of this system is calculated to be 228 in 1550 nm band, which is much larger than that of LSPR based sensors [29,30]. In addition, we examine the sensing performance using another wavelength of 800 nm ($H_{Si}$ is decreased to be 100 nm). Again the resonance shows a good linear dependence on $n_2$. In spite of a lower $Q$ of 680, a higher sensitivity (298 nm/RIU) and higher FOM (253) are achieved. These results demonstrate the feasibility and universality of this hybrid mode for RI sensing, no matter what wavelength is used. In practical sensing applications, appropriate wavelength band can be chosen to obtain a better sensing performance.

## 4. Hybrid plasmonic cavity-enhanced particle trapping

In the past decades, optical tweezers have developed into an indispensable tool for a variety of applications, such as nanoparticle trapping and manipulation, which are especially important for nanoparticle detection [31–33]. Traditional optical force is acted on particles using a tightly focused intense laser beam. Yet the device is relatively bulky, also with inefficient energy

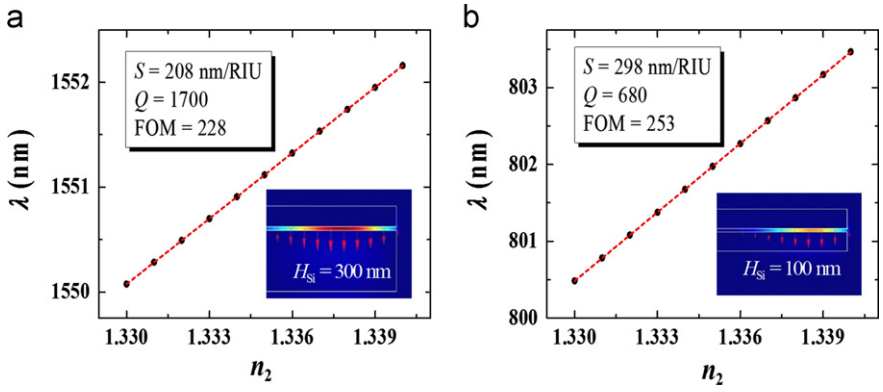


**Fig. 3.** Comparison of sensing performance for 1550 nm and 800 nm wavelength bands: (a) $\lambda=1550$ nm, $H_{Si}=300$ nm and (b) $\lambda=800$ nm, $H_{Si}=100$ nm; $n_2$ denotes the refractive index of the surrounding solution. The azimuthal mode numbers are $m=110$ for (a) and $m=180$ for (b).

utilization, while plasmonic structure is expected to be a promising candidate to realize a compact optical tweezer. In the following, we analyze the feasibility of this hybrid structure as an optical tweezer and the result shows that it can stably trap PS nanoparticles with considerably reduced input optical power.

For the nanometer-sized particle, we can treat it as a dipole, and the gradient force is calculated by [34,35]

$$F_{\text{grad}} = 4\pi\varepsilon_0 \frac{n_b{}^3 r^3}{2}\left(\frac{m^2-1}{m^2+2}\right)\nabla E^2 \tag{2}$$

where $m=n_p/n_b$, with $n_b$ and $n_p$ representing the refractive index of the surrounding medium and the nanoparticle whose radius is denoted by $r$. In our calculation, we take $n_b=1.33$ for water, $n_p=1.59$ for PS nanoparticle, and $r=5$ nm (typical size of a single protein molecule).

Fig. 4 plots the calculated quasi-Hooke gradient force experienced by a particle located in the middle of the gap. There exists at least one stable equilibrium point for particles under test. For stable trapping, it is generally required that the trapping potential $U > 10k_BT$. This condition is satisfied for all modes in Fig. 4. For a cavity with $R=1$ μm, the largest gradient force $F_x$ reaches as high as $-48$ pN/W, quite larger than that of a trapping system without cavity, which is typically several pN/W [20]. Therefore an optical potential as deep as $249k_BT$/W can be formed (Fig. 4(a)), which means with a moderate 40 mW input power, we can safely seize the nanoparticle. When the cavity becomes larger, the normalized potential will decrease because the power enhancement $G$ drops. In this condition, larger input power is required to establish a stable trapping. Yet, as larger cavity supports higher order modes, there can be multiple trapping tracks. For example, when the cavity radius increases to 3 μm, one (two) trapping potential well(s) can be formed in the 1st (2nd) order radial mode, as shown in Fig. 4(b,c). For an $R=5$ μm cavity, three radial modes are supported. As a result, three different numbers of trapping potential wells exist, as shown in Fig. 4 (d–f). With radial mode order increasing, although the gradient force at the rim of the cavity is always maximal, the position of the deepest potential well moves toward cavity center. This phenomenon can be used to control the trapping location of the nanoparticle by exciting different radial modes in this hybrid structure. It is also noted that the largest potential of the higher order mode does not decrease much. For instance, for the $R=3$ μm microcavity, the largest potential decreases from only $68k_BT$/W (the 1st order mode in Fig. 4(c)) to $50k_BT$/W (the 2nd order mode in Fig. 4(b)), while for $R=5$ μm microcavity, the largest potential stays almost unchanged from the 3rd order mode ($36k_BT$/W) to the 2nd order ($35k_BT$/W) and 1st order mode ($35k_BT$/W), as shown in Fig. 4(d) and (e). This is of practical significance, since the energy utility efficiency of the higher order mode is reasonably high enough, even if only the largest potential well is used for practical sensing.

To stably trap a particle, we must also consider the scattering force $F_{\text{scat}}$, which exerts a propulsion force to the nanoparticle along the light propagation direction, i.e. the tangential of the cavity edge. The force $F_{\text{scat}}$ can be estimated as [35]

$$F_{\text{scat}} = \frac{I_0}{c}\frac{128\pi^5 r^6}{3\lambda^4}\left(\frac{m^2-1}{m^2+2}\right)^2 n_b \tag{3}$$

For a small PS nanoparticle with radius of 5 nm considered here, the scattering force is about $1\times10^{-3}$ fN/$W$ in our device, which is negligible compared with the gradient force.

To further study the particle trapping ability, we calculate the particle distribution density $\rho(x)$ driven by the optical gradient force under thermal equilibrium. According to statistical mechanics, $\rho(x)$ should be proportional to$x$ exp[$-U(x)/k_BT$], where $U(x)$ is the energy potential formed by the optical force.

The distribution density of the trapped nanoparticle is shown in Fig. 5. It is clearly seen that with cavity radius increasing, more and more trapping regions appear, corresponding to several field intensity maximums. For example, when $R=1$ μm, only the fundamental radial mode is supported, so just one trapping region exists near the boundary of the cavity, as shown in Fig. 5(a). When $R$ increases to 3 (5) μm, two (three) radial modes are supported, and correspondingly, two (three) trapping regions appear, as shown in Fig. 5(b,c). This implies that the trapping location can be controlled through exciting different hybrid modes with different radial orders.

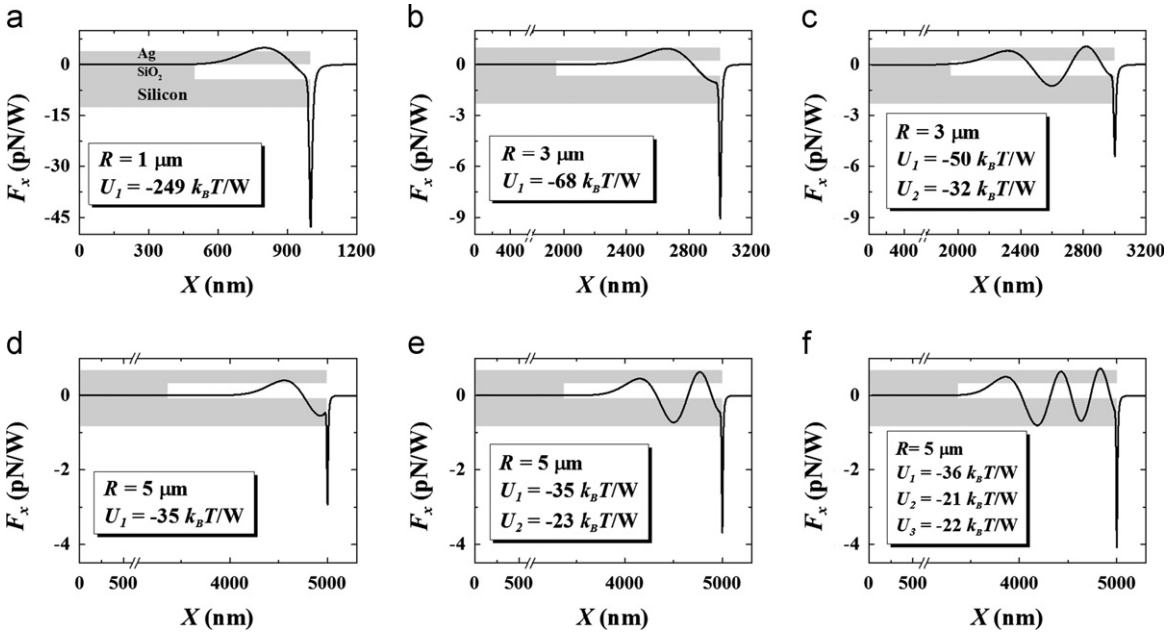


**Fig. 4.** Gradient force along the center line in the gap. $X=0$ denotes the center of the microdisk. All fundamental modes are around 1550 nm, and higher order modes have the same $m$ with corresponding fundamental modes. (a) Gradient force for the 1st-order radial mode for $R=1$ μm cavity (azimuthal mode number $m=9$). Gradient force for the 1st (b) and 2nd (c) order radial modes for an $R=3$ μm cavity ($m=31$). Gradient force for the 1st (d), 2nd (e), and 3rd (f) radial mode for an $R=5$ μm cavity ($m=53$). $U_i$ denotes the $i$th trapping potential well counting from left. The shadow areas mark the locations of the cavity.

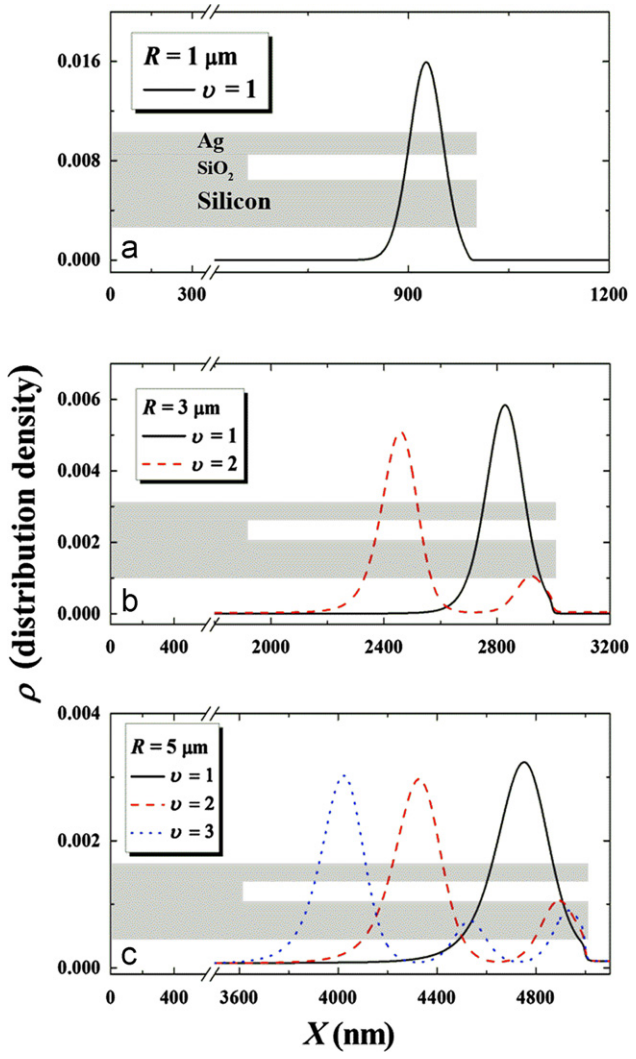


**Fig. 5.** Particle distribution density $\rho$ at different locations with 100 mW input power for $R$=1 μm (a), $R$=3 μm (b), and $R$=5 μm (c) cavities. For particle trapping, it is better to choose a small $R$=1 μm ($m$=9, $\upsilon$=1) cavity as $\rho$ is larger at the trapping spot. While for particle trapping position control, $R$=5 μm cavity can achieve greater displacement (~800 nm) when cavity mode is switched from $m$=53, $\upsilon$=1 mode to $m$=53, $\upsilon$=3 mode.

For example, for a cavity with radius of 5 μm, with 100 mW input power, about 800 nm position shift can be achieved (Fig. 5(c)) by switching the mode from the 1st to the 3rd order. For a greater particle displacement, a larger cavity is essentially required. This scheme could be useful for lab-on-a-chip applications [36].

## 5. Efficient coupling with a waveguide

For integrated optics applications, the energy exchange between a cavity and an external device in close proximity is of great interest. To realize an efficient coupling, the phase-matching condition should be satisfied. Here we consider the excitation of the hybrid modes with a silicon waveguide. The mode index of the cavity can be obtained by applying $n_c = m\lambda/2\pi R_c$. If we approximately take $R$ as $R_c$, then the cavity mode index $n_c$ can be calculated from Table 1, as shown in Fig. 6 (black solid line). It should be noted that the real $n_c$ is a little larger than that in our estimation since $R_c$ is a little smaller than $R$.

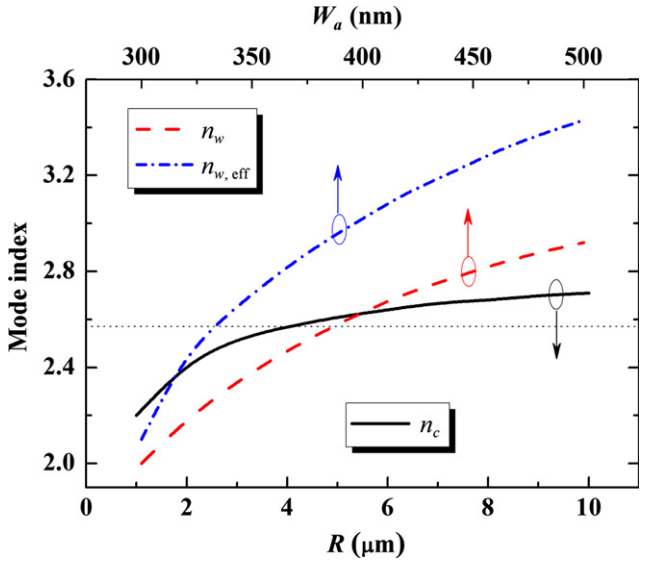


**Fig. 6.** Cavity mode index $n_c$ (black solid line) with different $R$, waveguide mode index $n_w$ (red dashed line) and effective waveguide mode index $n_{w,eff}$ (blue dash dotted line) with different $W_a$. To achieve efficient coupling, $n_c = n_{w,eff}$ should be satisfied. For example, when $R$=4 μm and $W_a$=330 nm, the cavity and waveguide modes can be well matched ($n_c = n_{w,eff} \sim 2.6$, see black dotted line). Structure size parameters: $H_{Ag}$=100 nm, $g$=20 nm and $W_a$=100 nm. (For interpretation of the references to color in this figure legend, the reader is referred to the web version of this article.)

When the cavity mode is coupled by a waveguide, it should be noted that an effective mode index $n_{w,eff}$, instead of the realistic waveguide mode index $n_w$, should match the cavity mode index $n_c$, because of the curved and straight geometries of the cavity and waveguide [37]. The effective mode index of the waveguide is calculated by

$$n_{w,eff} = n_w\left(1 + \frac{D}{2R}\right) \tag{4}$$

where $D = W_g + W_a/2$ (see Fig. 1). The waveguide mode index $n_w$ and effective waveguide mode index $n_{w,eff}$ with different $W_a$ are shown in the red dashed and blue dash dotted curves in Fig. 6, respectively. It can be seen that, for a given cavity, the hybrid mode in this structure can always be effectively excited with an appropriate waveguide.

## 6. Conclusion

In summary, we have investigated the properties of a hybrid photonic–plasmonic microdisk cavity and its applications in RI sensing and nanoparticle trapping. $Q$ factor as high as ~2000 is achieved despite the existence of metallic loss. Its application as a high performance refractometer with sensitivity larger than 200 nm/RIU and FOM higher than 200 is obtained. Furthermore, with the compact field enhancement, the optical gradient force can be substantially magnified, thus providing a promising platform for nanoparticle trapping as optical tweezers. In addition, taking advantage of the multi-mode in this hybrid microcavity, selective trapping tracks can be realized. Finally, we show that, with a silicon waveguide, the hybrid mode in this photonic–plasmonic structure can be effectively excited, which paves the way for practical applications of this type of device in a nano-photonic integrated circuit.

## Acknowledgments

The authors acknowledge financial support from the National Natural Science Foundation of China under Grant nos. 11004003, 11121091 and 11222440, and 973 program (No. 2013CB328704). Y.F.X. was also supported by the Research Fund for the Doctoral Program of Higher Education (No. 20090001120004). Y.X.L. was supported by the National Fund for Fostering Talents of Basic Science (Nos. J1030310 and J1103205) and the Chun-Tsung Scholar Fund for Undergraduate Research of Peking University.

## References

1 K.J. Vahala, Nature 424 (2003) 839.
2 F. Vollmer, D. Braun, A. Libchaber, M. Khoshsima, I. Teraoka, S. Arnold, Applied Physics Letters 80 (2002) 4057.
3 E. Krioukov, D.J.W. Klunder, A. Driessen, J. Greve, C. Otto, Optics Letters 27 (2002) 512.
4 N.M. Hanumegowda, C.J. Stica, B.C. Patel, I. White, X. Fan, Applied Physics Letters 87 (2005) 201107.
5 H. Yi, D.S. Citrin, Y. Chen, Z. Zhou, Applied Physics Letters 95 (2009) 191112.
6 J. Zhu, S.K. Ozdemir, Y.-F. Xiao, L. Li, L. He, D.-R. Chen, L. Yang, Nature Photonics 4 (2009) 46.
7 T. Lu, H. Lee, T. Chen, S. Herchak, J.-H. Kim, S.E. Fraser, R.C. Flagen, K. Vahala, Proceedings of the National Academy of Sciences of the United States of America 108 (2011) 5976.
8 R. Ameling, L. Langguth, M. Hentschel, M. Mesch, P.V. Braun, H. Giessen, Applied Physics Letters 97 (2010) 253116.
9 M. Barth, S. Schietinger, S. Fischer, J. Becker, N. Nüsse, T. Aichele, B. Löchel, C. Sönnichsen, O. Benson, Nano Letters 10 (2010) 891.
10 M.A. Santiago-Cordoba, S.V. Boriskina, F. Vollmer, M.C. Demirel, Applied Physics Letters 99 (2011) 073701.
11 S.I. Shopova, R. Rajmangal, S. Holler, S. Arnold, Applied Physics Letters 98 (2011) 243104.
12 M.A. Santiago-Cordoba, M. Cetinkaya, S.V. Boriskina, F. Vollmer, M.C. Demirel, Journal of Biophotononics 5 (2012) 629.
13 W. Ahn, S.V. Boriskina, Y. Hong, B.M. Reinhard, ACS Nano 6 (2012) 951.
14 Y.-F. Xiao, Y.-C. Liu, B.-B. Li, Y.-L. Chen, Y. Li, Q. Gong, Physical Review A 85 (2012) 031805(R).
15 R.F. Oulton, V.J. Sorger, D.A. Genov, D. Pile, X. Zhang, Nature Photononics 2 (2008) 496.
16 B. Yun, G. Hu, Y. Ji, Y. Cui, Journal of the Optical Society of America B: Optical Physics 26 (2009) 1924–1929.
17 M.Z. Alam, J. Meier, J.S. Aitchison, M. Mojahedi, Optics Express 18 (2010) 12971.
18 J.T. Kim, J.J. Ju, S. Park, M. Kim, S.K. Park, S.Y. Shin, Optics Express 18 (2010) 2808.
19 X. Yang, A. Ishikawa, X. Yin, X. Zhang, ACS Nano 5 (2011) 2831.
20 X. Yang, Y. Liu, R.F. Oulton, X. Yin, X. Zhang, Nano Letters 11 (2011) 321.
21 Y.-F. Xiao, B.-B. Li, X. Jiang, X. Hu, Y. Li, Q. Gong, Journal of Physics B: Atomic, Molecular and Optical Physics 43 (2010) 035402.
22 Y.-F. Xiao, C.-L. Zou, B.-B. Li, Y. Li, C.-H. Dong, Z.-F. Han, Q. Gong, Physical Review Letters 105 (2010) 153902.
23 D. Dai, Y. Shi, S. He, L. Wosinski, L. Thylen, Optics Express 19 (2011) 23671.
24 X. Yu, L. Shi, D. Han, J. Zi, P.V. Braun, Advanced Functional Materials 20 (2010) 1910.
25 M. Chamanzar, M. Soltani, B. Momeni, S. Yegnanarayanan, A. Adibi, Applied Physics B: Lasers and Optics 101 (2010) 263.
26 Y. Song, J. Wang, M. Yan, M. Qiu, Journal of Optics–Nouvelle Revue D Optique 13 (2011) 075001.
27 L. Zhou, X. Sun, X. Li, J. Chen, Sensors 11 (2011) 6856.
28 N. Verellen, P. Van Dorpe, C. Huang, K. Lodewijks, G.A.E. Vandenbosch, L. Lagae, V.V. Moshchalkov, Nano Letters 11 (2011) 391.
29 J.N. Anker, W.P. Hall, O. Lyandres, N.C. Shah, J. Zhao, R.P. Van Duyne, Nature Materials **7** (2008) 442.
30 K. Lodewijks, W. Van Roy, G. Borghs, L. Lagae, P. Van Dorpe, Nano Letters 12 (2012) 1655.
31 A. Ashkin, J.M. Dziedzic, T. Yamane, Nature 330 (1987) 769.
32 M.M. Wang, E. Tu, D.E. Raymond, J.M. Yang, H. Zhang, N. Hagen, B. Dees, E.M. Mercer, A.H. Forster, I. Kariv, Nature Biotechnology 23 (2004) 83.
33 M.P. MacDonald, G.C. Spalding, K. Dholakia, Nature 426 (2003) 421.
34 P.W. Smith, A. Ashkin, W.J. Tomlinson, Optics Letters 6 (1981) 284.
35 A. Ashkin, J.M. Dziedzic, J.E. Bjorkholm, S. Chu, Optics Letters 11 (1986) 288.
36 S. Haeberle, R. Zengerle, Lab on a Chip **7** (2007) 1094.
37 D.R. Rowland, and J.D. Love, Evanescent wave coupling of whispering gallery modes of a dielectric cylinder , IEE Proceedings Journal of Optoelectronics, 140(3) pp. 177–188 1993.